






Strong gravitational lensing by AGNs as a probe of the quasar–host relations in the distant Universe

Received: 10 March 2022

Accepted: 26 April 2023

Published online: 01 June 2023

 Check for updates

Martin Millon ^{1,2}✉, Frédéric Courbin ¹, Aymeric Galan ^{1,3},
Dominique Sluse ⁴, Xuheng Ding⁵, Malte Tewes ⁶ & S. G. Djorgovski⁷

The tight correlations found between the mass of supermassive black holes and the luminosities, stellar masses and velocity dispersions of their host galaxies are often interpreted as a sign of their co-evolution. Studying these correlations across redshift provides a powerful insight into the evolutionary path followed by the quasar and its host galaxy. While the mass of the black hole is accessible from single-epoch spectra, measuring the mass of its host galaxy is challenging as the active nucleus largely overshines its host. Here we present a technique to probe quasar–host relations beyond the local Universe with strong gravitational lensing, hence overcoming the use of stellar population models or velocity dispersion measurements, both prone to degeneracies. We study in detail one of the three known cases of strong lensing by a quasar to accurately measure the mass of its host and to infer a total lensing mass within the Einstein radius. The lensing measurement is more precise than any other alternative technique and compatible with the local scaling relation between the mass of the black hole and the stellar mass. The sample of such quasar–galaxy or quasar–quasar lensing systems should reach a few hundred with Euclid and the Rubin-Large Synoptic Survey Telescope, thus enabling the application of such a method with statistically significant sample sizes.

We present an exceptional case of strong lensing by an elliptical galaxy displaying a well-visible substructure pointed to us by a quasar: SDSS J0919 + 2720 (ref. 1). The elliptical galaxy and SDSS J0919 + 2720 share the same redshift ($z_l = 0.209$), are separated by less than $1''$ on the plane of the sky and act as a gravitational lens on a distant star-forming source at $z_s = 0.558$. Most of the lensing effect is produced by the main elliptical lens galaxy (Fig. 1), but the quasar and its host galaxy, even hidden in the glare of the quasar light, produce detectable lensing signal. We take advantage of this fortunate lensing event and of the fact that the

quasar and the main elliptical lensing galaxy do not share the same location to measure the total (dark + luminous) mass of a quasar host galaxy with strong gravitational lensing.

Quasars are known to follow tight correlations between the mass of their central supermassive black hole (SMBH) and the fundamental properties of their host galaxy, such as the stellar mass $M_{*,h}$ and stellar velocity dispersion $\sigma_{*,h}$ related to the total mass $M_{\text{Tot},h}$. The very existence of these scaling relations suggests a connection between the quasar activity and the formation of its host galaxy (see, for example,

¹Institute of Physics, Laboratory of Astrophysics, École Polytechnique Fédérale de Lausanne (EPFL), Versoix, Switzerland. ²Kavli Institute for Particle Astrophysics and Cosmology and Department of Physics, Stanford University, Stanford, CA, USA. ³Department of Physics, TUM School of Natural Sciences, Technical University of Munich, Garching, Germany. ⁴STAR Institute, Liège, Belgium. ⁵Kavli Institute for the Physics and Mathematics of the Universe, University of Tokyo, Kashiwa, Japan. ⁶Argelander-Institut für Astronomie, Universität Bonn, Bonn, Germany. ⁷California Institute of Technology, Pasadena, CA, USA. ✉e-mail: martin.millon@epfl.ch

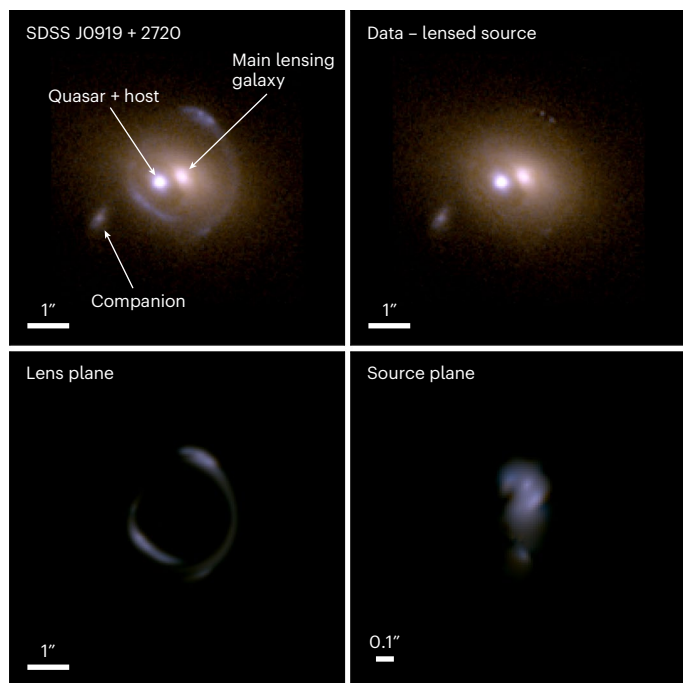


Fig. 1 The SDSS J0919 + 2720 strongly lensed system. Top left: Colour composite of the HST images in the F475W and F814W bands. The different components of the system are indicated: the main lensing elliptical galaxy at $z = 0.209$ produces most of the lensing effect on the (blue) star-forming galaxy at $z = 0.558$. The bright blue quasar and its host galaxy, also at $z = 0.209$, act as a secondary deflector for which we can measure the total mass. Top right: HST image, where the best-fit model of the gravitational arcs has been subtracted. Bottom left: Best-fit model of the lensed arcs. Bottom right: Source reconstruction using wavelet decomposition and sparse regularization. The pixel size is $0.013''$, three times smaller than the drizzled HST images (see Methods for more detail on the lens modelling).

refs. 2,3). The physical process leading to these correlations remains unclear since the gravitational influence of the SMBH is limited to parsec scales while the typical scale of their host galaxy is three orders of magnitude larger. On the one hand, active galactic nuclei (AGN) feedback in numerical simulations seems to reproduce the observed correlations (see, for example, refs. 4,5), but on the other hand, they could also simply result from the hierarchical assembly of multiple mergers (see, for example, ref. 6). Discriminating between these scenarios requires measuring the bulge mass of quasar host galaxies not only in the local Universe but also at higher redshift, where velocity dispersion measurements are challenging but where lensing is both precise and accurate. If the scatter in the $M_{\text{BH}} - M_{\text{Tot,h}}$ relation (where M_{BH} is the mass of the black hole) increases with redshift, this would support the hierarchical assembly scenario⁷.

Moreover, it is not well established if there is an offset between the relations observed in the local and high-redshift Universe. For example, Sexton et al.⁸ did not find any evidence for an evolution of the $M_{\text{BH}} - \sigma_{*,\text{h}}$ relation with redshift. On the other hand, recent works by Ding et al.^{9,10} found a positive evolution of the $M_{\text{BH}}/M_{*,\text{h}}$ ratio, compatible with a scenario where the SMBH would grow at an earlier time and the bulge of its host galaxy is catching up later. If both of these results are correct, this would imply that the bulge stellar mass increases without substantially changing the total mass of the galaxy. Possible mechanisms leading to the growth of the bulge without increasing the black hole mass nor the total mass would involve a transfer of stellar mass from the disk to the bulge through minor mergers or disk instabilities^{11,12}. The absence of evolution in the $M_{\text{BH}} - \sigma_{*,\text{h}}$ relation (see, for example, refs. 8,13) suggests that the offset found in earlier works (for example, refs. 14,15)

could result from selection effects on both M_{BH} and $\sigma_{*,\text{h}}$. In that case, the absence of change in these scaling relations across cosmic time would thus indicate a close co-evolution between the SMBH and its host, possibly regulated through AGN feedback or because they share a common gas reservoir¹⁶.

All these studies are currently limited by the difficulty of measuring $M_{*,\text{h}}$ and $\sigma_{*,\text{h}}$ at high redshift because of deblending issues between the quasar and stellar emission, uncertainties on the initial mass function (IMF) and selection effects due to the luminosity selection process involved in most quasar samples (see, for example, ref. 17). Additionally, converting $\sigma_{*,\text{h}}$ into $M_{\text{Tot,h}}$ requires breaking the mass–anisotropy degeneracy. This can be achieved by using spatially resolved kinematics measurements, but these are very difficult in the distant Universe because the quasar is often brighter than the stellar component. In summary, measuring the total and stellar mass of the host both faces important observational challenges and relies on questionable assumptions. In this Article, we propose a technique based on gravitational lensing to measure the total mass of the host with excellent precision, which also imposes a strict upper limit on the stellar mass within the Einstein radius.

SDSS J0919 + 2720 provides a test bench to carry out the experiment, at redshift $z = 0.209$. It is one of the three known cases of lensing by a quasar discovered by Courbin et al.¹. Other candidates were proposed in early searches by Claeskens et al.¹⁸ and more recently by Meyer et al.¹⁹, but they have not yet been confirmed by high-resolution imaging. Among these three confirmed systems, SDSS J0919 + 2720 is the only type I AGN displaying well-visible gravitational arcs. This paper presents an analysis of such a system, where the lensing (total) mass, the host stellar mass and the black hole mass are measured. SDSS J0919 + 2720 is, for now, the most striking case of lensing by a quasar, but a few hundred will be found in the near future by wide-field imaging surveys²⁰, opening the path to measure robust scaling relations up to redshifts close to $z = 1$, that is, well beyond the local Universe. Although SDSS J0919 + 2720 requires complex lens models to disentangle the mass of the quasar host from the mass of the nearby massive elliptical galaxy, most future cases of lensing by a quasar should be massive enough to produce an Einstein ring by themselves²⁰, allowing us to obtain a straightforward and model-independent measurement of the lensing mass directly from the Einstein radius.

Throughout this paper, we assume a flat- Λ cold dark matter cosmology with the Hubble constant, $H_0 = 70 \text{ km s}^{-1} \text{ Mpc}^{-1}$, the matter density, $\Omega_m = 0.3$, and the energy density due to the cosmological constant, $\Omega_\Lambda = 0.7$. These cosmological parameters are used to compute the angular diameter distances from the redshifts measurements. We adopt the AB magnitude system.

Results

Lensing mass estimates

We use Hubble Space Telescope (HST) images (program GO-12233; PI Courbin) of SDSS J0919 + 2720 taken in the F475W and F814W optical bands to reconstruct the total mass distribution of the system. Because the positions of the quasar host and that of the main lens do not coincide, our lens models are able to separate the total mass of the quasar and its host from that of the main elliptical lensing galaxy. To perform the modelling, we fit simultaneously the two HST bands, imposing that the light and mass profiles in the lens plane share the same centre in both bands and fixing their position during the fit.

Following common practice for strong lens models, we describe the mass of the main lens galaxy as a power-law elliptical mass distribution (PEMD) whose slope, γ_l , can vary during the fit. For the mass of the quasar host galaxy, we consider a singular isothermal ellipsoid (SIE), which by definition has a fixed slope of $\gamma_{\text{host}} = 2$. We do not consider any explicit point-mass component for the quasar mass as it is negligible in front of the mass of its host. The light of the source galaxy is reconstructed with shapelets, leading to 103 linear parameters, directly

Table 1 | ΔBIC , total mass of the quasar host galaxy, $M_{\text{Tot,h}}$ and $\Delta\chi^2_{\text{img}}$ for different lens modelling assumptions

Model main lens galaxy	Model quasar host galaxy	Model companion galaxy	ΔBIC	$\log_{10}\left(\frac{M_{\text{Tot,h}}}{M_{\odot}}\right)$	$\Delta\chi^2_{\text{img}}$
PEMD	SIE	—	0	$10.27^{+0.06}_{-0.07}$	0.00
PEMD	PEMD	—	4	$10.30^{+0.07}_{-0.05}$	-1.08×10^{-4}
SIE	SIE	—	9	$10.03^{+0.05}_{-0.06}$	5.72×10^{-4}
PEMD	NIE + point mass	—	23	$10.27^{+0.07}_{-0.08}$	5.07×10^{-5}
PEMD	Point mass	—	25	$10.08^{+0.06}_{-0.06}$	7.07×10^{-4}
PEMD	SIE	SIE	66	$10.17^{+0.15}_{-0.16}$	-1.80×10^{-4}
PEMD	—	—	234	—	6.35×10^{-3}

ΔBIC and $\Delta\chi^2_{\text{img}}$ are computed relative to our baseline model that describes the main lensing galaxy as a PEMD and the quasar host as an SIE.

optimized from the inversion of the lens equation, and 18 non-linear free parameters simultaneously optimized in a Bayesian framework. Our best-fit model is presented in Fig. 1. As a final step, we perform a fully non-parametric reconstruction of the source, for the best-fit mass model, on a pixelated grid regularized with wavelets²¹. This leads to a high-resolution image of the star-forming source galaxy.

As the quasar host is not centred on the main lens galaxy, our models have high sensitivity to its mass and we can measure it in a very robust way. Our best model provides its Einstein radius $\theta_{\text{E,h}} = 0.355''^{+0.024}_{-0.028}$, which translates into a total mass of $\log_{10}(M_{\text{Tot,h}}/M_{\odot}) = 10.27^{+0.06}_{-0.07}$ within the Einstein radius of 1.2 kpc in the lens plane. Models generated with and without including the quasar host galaxy have a very different Bayesian information criterion (BIC), with $\Delta\text{BIC} = 234$ (see Table 1 and Methods for alternative modelling assumptions). This strongly favours models with explicit modelling of the substructure marked by the quasar and shows that we have high sensitivity to it. We also measure the Einstein radius of the main galaxy, $\theta_{\text{E,m}} = 1.016''^{+0.016}_{-0.016}$, corresponding to a total mass of $\log_{10}(M_{\text{Tot,m}}/M_{\odot}) = 11.18^{+0.01}_{-0.01}$ within a radius of 3.5 kpc. Our lens model predicts a luminosity-weighted line-of-sight velocity dispersion (as described in ref. 22) of $\sigma_{*,h} = 111 \pm 3 \text{ km s}^{-1}$ for the quasar host galaxy and of $\sigma_{*,m} = 227 \pm 3 \text{ km s}^{-1}$ for the main galaxy. These estimates are obtained by solving the spherical Jeans equations, assuming isotropic motion of the stars. They are given here for reference, only as a dynamical equivalent of the lensing measurement.

As an additional test, we verify the robustness of the fit by optimizing a series of models with fixed $M_{\text{Tot,h}}$ in the range $10^6 M_{\odot} < M_{\text{Tot,h}} < 10^{12} M_{\odot}$. For each value of $M_{\text{Tot,h}}$ we re-optimize all other free parameters, including the source reconstruction, and we check whether the new model optimization and source reconstruction compensate for the variations introduced in the image plane. We then compute the corresponding value of ΔBIC to determine whether the changes seen in the image residuals are statistically significant. Figure 2 illustrates this process and shows a minimum in ΔBIC for $\log_{10}(M_{\text{Tot,h}}/M_{\odot}) = 10.27$, which also happens to be the value we find when optimizing models where $M_{\text{Tot,h}}$ is free. The plateau seen until $M_{\text{Tot,h}} < 10^8 M_{\odot}$ can be interpreted as our detection threshold. This plateau provides similar information to the sensitivity maps of Despali et al.²³ and indicates that we are sensitive to masses on the order of 10^8 – $10^9 M_{\odot}$, at the position of the quasar. This is excellent given that the quasar is not located right on the lensed image of the source, where mass sensitivity would be even better.

Stellar and black hole mass estimates

Strong lensing provides us with $M_{\text{Tot,h}}$, but the HST images also give access to the stellar light of the quasar host, which we use to estimate its stellar mass, $M_{*,h}$. This requires to model and remove the quasar

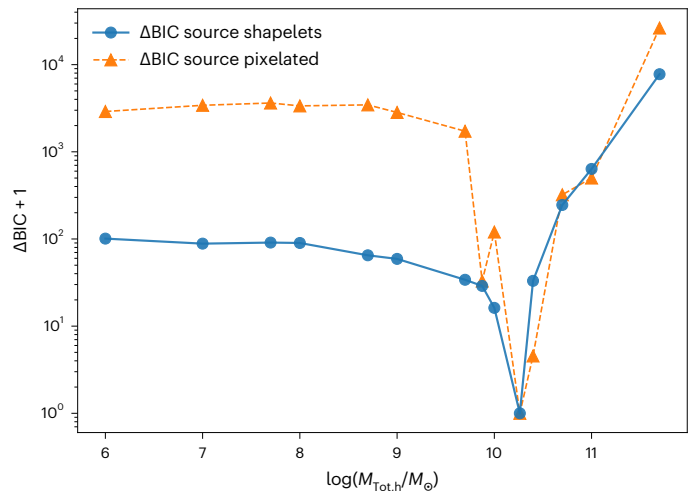


Fig. 2 | Value of ΔBIC for different masses of the quasar host galaxy, with a clear minimum for host total mass of $\log_{10}(M_{\text{Tot,h}}/M_{\odot}) = 10.27$. The results for models with (analytic) shapelet decomposition of the source and fully pixelated source regularized with wavelets. The ΔBIC values are computed relative to the best model for each source reconstruction method. Note that the two corresponding curves do not overlap other than at the minimum because the two types of models have very different numbers of degrees of freedom. Still, the positions of the minima agree well, showing that our results are robust against the source reconstruction method.

light and therefore to model the instrumental point spread function (PSF) accurately. We do this by using HST images of the open cluster NGC 136, taken close in time to the observations of SDSS J0919 + 2720 and with the same dithering pattern. This young cluster allows us to build a model of the PSF using blue stars with colours matching that of the quasar and close to its position on the detector.

We fit our PSF model at the quasar position as well as a model for the light component of the main lensing galaxy and of the quasar host galaxy. We measure the quasar host flux in an aperture of $0.71''$ in diameter, corresponding to twice the Einstein radius of the quasar host. The modelling of the colour of the host ($F475W - F814W = 1.09 \text{ mag}$) translates into a stellar mass of $\log_{10}(M_{*,h}/M_{\odot}) = 9.80$, assuming a Chabrier IMF and solar metallicity. The typical uncertainty on the stellar mass is 0.2 dex, similar to ref. 9. Comparing this number with the total lensing mass within an aperture of $0.71''$ (2.4 kpc in diameter in the lens plane), we infer a stellar to total mass ratio $M_{*,h}/M_{\text{Tot,h}}$ of 0.34 ± 0.27 . The stellar mass of the main galaxy $M_{*,m}$ is estimated in a similar way, that is, from photometry within an aperture of $2.03''$, corresponding to twice the Einstein radius of the main lens. We infer $\log_{10}(M_{*,m}/M_{\odot}) = 10.72$ for Chabrier IMF.

Finally, we compare the stellar and lensing masses with the black hole mass M_{BH} . SDSS J0919 + 2720 has been observed as part of the Sloan Digital Sky Survey (SDSS) and with the Low Resolution Imaging Spectrometer (LRIS) on the Keck Telescope¹. Both spectra show prominent broad emission lines in the optical, making it possible to estimate the virial mass of the central black hole via the so-called single-epoch method. Using the measured width of the broad H α line and the continuum flux at 6,200 Å, we found a black hole mass of $\log_{10}(M_{\text{BH}}/M_{\odot}) = 7.32$ from the Keck spectrum and $\log_{10}(M_{\text{BH}}/M_{\odot}) = 7.29$ from the SDSS spectrum, with 0.35 dex uncertainties.

Figure 3 shows how SDSS J0919 + 2720 compares with other local AGNs in the $M_{\text{BH}} - M_{*,h}$ plane. The points corresponding to the stellar mass inferred from photometry of the quasar host or from lensing are well on the correlation. Both masses are measured in an aperture of 2.4 kpc, matching the Einstein radius of the quasar host. The stellar mass and total mass estimates do not differ by more than a factor of 3.

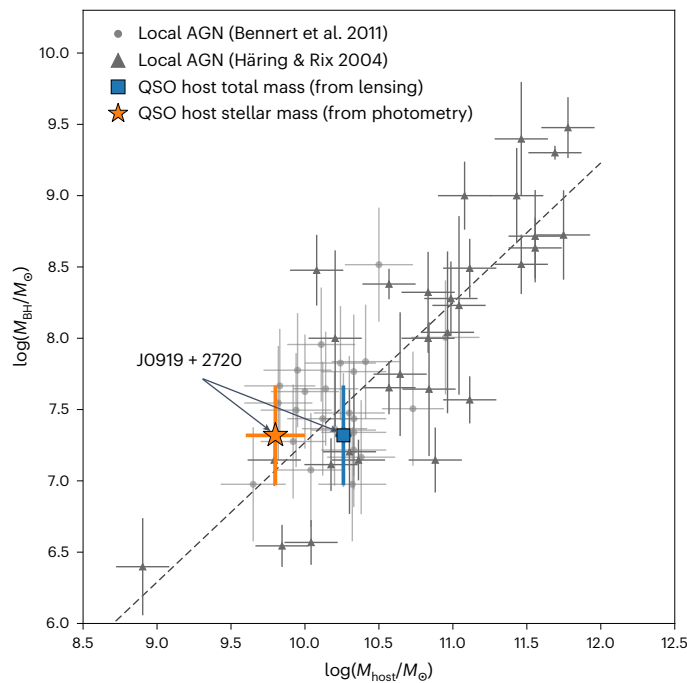


Fig. 3 | $M_{\text{BH}}-M_{\text{h}}$ relation for local ($z \lesssim 0.08$) AGNs taken from refs. 48,49 (grey points). Our total mass estimates from lensing and our stellar mass estimates from photometry (assuming Chabrier IMF), for the quasar host galaxy in the SDSS J0919 + 2720 system. The dashed line indicates the best-fit local relation. Data presented as the median of the posterior distribution, and error bars correspond to the 16th and 84th percentiles.

Discussion

Scaling relations between the mass of quasars and that of their host galaxies are a powerful diagnostic of their co-evolution. A change of the relations with redshift may well indicate a change in time of the physical processes at play in quasar and galaxy formation and co-evolution⁷. But for this to work, scaling relations must be established reliably, ideally with one single method and over a broad redshift range.

Building scaling laws is notoriously difficult as it involves measurements of the mass of the central black hole from emission line properties of the quasar and the mass of the host galaxy. The black hole mass estimate involves assumptions on the geometry and dynamics of the emitting material producing the lines and “measuring the mass of the host galaxy is trickier than it sounds”⁷. Using multi-band photometry allows us to estimate its stellar mass with fairly large error bars as this requires assumptions on the stellar populations of the host, its metallicity and a choice of the IMF. Turning the stellar mass into a total mass further assumes a mass-to-light ratio, not to mention that this ratio may well be spatially variable across the galaxy.

Alternatively, the total mass can be estimated through a stellar velocity dispersion measurement, provided the host galaxy can be seen in the glare of the much brighter quasar. Although this has been attempted in the past with HST and ground-based adaptive optics²⁴ or even in spectroscopy with the Very Large Telescope²⁵, the method becomes very difficult with increasing redshift. In addition, the interpretation of the velocity dispersion itself depends on all the above assumptions on photometric stellar masses but also requires assumptions on the light profile of the host galaxy. For this reason, scaling relations using velocity information have been limited so far to local or intermediate redshift ($z \approx 0.5$) quasar host galaxies (see, for example, ref. 8).

Strong gravitational lensing offers an extremely valuable alternative to measure the total mass of quasar host galaxies independent of any of the above assumptions: lensing measures the total mass in the Einstein radius, which is a very well-defined aperture. SDSS J0919 + 2720

provides the first clear case of a quasar acting as a gravitational lens on a more distant galaxy. We test a range of lensing models and find that our mass estimates are robust and little affected by systematic errors. We measure a total mass of $\log_{10}(M_{\text{Tot,h}}/M_{\odot}) = 10.27^{+0.06}_{-0.07}$ within 2.4 kpc with 16% precision. An additional source of error may come from line of sight (LOS) structures. We could potentially misattribute the mass within the Einstein radius to the host galaxy whereas it comes from a LOS structure. However, it has been demonstrated on a sample of time delay lenses by the TDCOSMO collaboration that this effect does not exceed a few percent and can be accurately corrected²⁶. Moreover, the lensed sources in this sample are at a much higher redshift ($z_s = 1.5-2.5$) than our source galaxy at a redshift of 0.55. These time delay systems are probably much more affected by LOS effects than our low-redshift lensed source. In the case of SDSS J0919 + 2720, we can expect that LOS effects are negligible and gravitational lensing thus much more precise than any other existing techniques. Our measurement is well compatible with scaling relations established in the local Universe, and given the small size of the Einstein radius, we measure mostly the bulge total mass. We note that lensing is probing a different quantity than $M_{\text{*h}}$ or even $\sigma_{\text{*h}}$ since the lensing mass is sensitive to the total projected mass in a cylinder. It can be related to $M_{\text{*h}}$ by assuming a mass-to-light ratio or to $\sigma_{\text{*h}}$ by solving the Jeans equation, assuming spherical symmetry of the mass distribution. Consequently, comparing how this lensing mass scales with the black hole mass is well complementary to the other scaling relations and will help to build a consistent picture among the different galaxy evolution scenarios.

As lensing is not affected by the same errors as traditional techniques, it might solve the question of the presence or not of an evolution of the $M_{\text{BH}}/M_{\text{Tot,h}}$ ratio over redshifts. Such evolution was not detected in the $M_{\text{BH}}-\sigma_{\text{*}}$ relation in ref. 8, up to redshifts of approximately 0.6, contradicting results found by previous studies^{14,15}. Lensing could settle this debate by measuring the total mass of the host on a similar redshift range, hence discriminating between (1) a scenario where the black hole grows first and is caught up by its host galaxy to end up on the relation observed locally and (2) a scenario where the two components co-evolve together, with tight control of the growth of the host, possibly via AGN feedback. We, therefore, propose to use strong lensing to establish the scaling laws involving the total mass of the host galaxy. Not only will this complement other techniques based on pure stellar mass measurements but it will also enable us to trace the evolution of the stellar-to-total mass ratio of quasar host galaxies.

SDSS J0919 + 2720 is only one case of strong lensing by a quasar, but the present detailed study with sharp HST images lends considerable hope to build scaling relations using reliable total masses with no strong astrophysical assumptions and at redshift typical for lensing galaxies, that is, up to $z = 1$. We emphasize that this method does not require the special geometrical configuration of SDSS J0919 + 2720, where the quasar is seen as a lensing substructure of the main deflector. This configuration simply enlarges the Einstein radius and increases the lensing magnification of the background source, which has made this system easier to detect. However, more massive quasar host galaxies are able to produce a detectable Einstein ring by themselves. Recent work²⁰ predicts the discovery of 80 such systems in the Hyper Suprime-Cam wide survey and several hundred of them in future large sky surveys such as Euclid and the Rubin-Large Synoptic Survey Telescope. Euclid will certainly be the best place to look for such objects as the instrumental PSF of 0.2” is two or three times smaller than the typical Einstein radius of a (quasar host) galaxy, hence drastically improving the light contrast between the foreground quasar and the background lensed source. Euclid will also have sufficient image resolution to obtain precise mass estimates directly from the survey data. The follow-up data needed to study the $M_{\text{BH}}-M_{\text{Tot,h}}$ relation with this technique will therefore be reduced to a single spectrum to measure the black hole mass, which can easily be obtained from ground-based 3 m class telescopes.

When a sample of quasi-stellar object (QSO) lenses becomes available, the main limitation in studying the $M_{\text{BH}}-M_{\text{Tot,h}}$ relation will be the uncertainty on the black hole mass, which currently reaches approximately 0.3 dex. The uncertainty on the total mass obtained with lensing will be negligible in comparison. However, the accuracy of black hole mass measurements in the distant Universe will continue to improve as more measurements become available from reverberation mapping (see, for example, refs. 27,28). These estimates can then be used to calibrate measurements from single-epoch spectroscopy. Finally, we expect that a large sample of quasar–galaxy and quasar–quasar lenses, comparable in size to all previous samples with velocity dispersions, will become accessible in the next decade and allow us to robustly determine the $M_{\text{BH}}-M_{\text{Tot,h}}$ relation across cosmic time.

Methods

HST observations, data reduction and PSF measurement

Our HST data consist of six consecutive dithered exposures with the F475W and F814W filters from the Wide Field Camera 3 instrument on board HST. The total exposure time of the combined drizzled frames is 2,274 and 2,382 s in the F475W and F814W band, respectively, with pixel scale of 0.04". The noise level at each pixel position is estimated from a Poisson noise component, scaled by the exposure map, and a background noise component, estimated from an empty region of the image by using *SExtractor*²⁹. The PSF is not built from the stars in the field of view of SDSS J0919 + 2720 but rather from the observation of the open star cluster NGC136 that was observed for one full orbit 4 months before SDSS J0919 + 2720. Blue stars with the same colour as SDSS J0919 + 2720 fall close to the quasar position on the charge-coupled device (CCD) camera and allow us to reconstruct an exquisite PSF with properties very close to the PSF of the quasar. This is crucial to deblend the quasar host galaxy from the point source component. Three long exposures of 350 s each and one short exposure of 60 s were taken using both filters. We use *SExtractor* on the dithered images to perform the photometry of all sources, and we select the stars within 1' from the position on the detector of SDSS J0919 + 2720. We then keep all stars that have an F475W–F814W colour matching that of the quasar within 0.5 mag. We further restrict our selection to sources in the magnitude range of 17.5–24.5 (18–25) in the F814W (F475W) band. We ensure that the selected sources are point-like objects by removing all sources with ellipticity larger than $\epsilon = 0.9$ and full width at half maximum (FWHM) larger than 2.8 pixels (0.11"). Finally, we visually inspect the cutouts of the selected stars and remove any star with companions. This results in respectively 12 and 9 useful stars in the F475W and F814W band. The stars are then stacked using the publicly available Python package *AstroObjectAnalyser* (<https://github.com/sibirrer/AstroObjectAnalyser>) to obtain a high signal-to-noise model of the PSF as well as an estimate of the PSF errors at each pixel position.

Lens modelling

We use the Python strong lens modelling public package *Lenstronomy*³⁰ that implements parametric models for the mass distribution of the lens as well as flexible shapelet-based reconstruction of the source. We fit the images in the F475W and F814W band jointly. That is, the mass profiles in the models are the same in both bands.

We model the lens light with two analytical Sérsic models at the position of the main lens galaxy sharing the same centroid position. The quasar light emission is modelled with a point source plus two Sérsic profiles at the position of the quasar host. The centroid of the two Sérsics are tied together and to the point source position. We add a Sérsic profile to fit the light of the companion galaxy lying at the south-east of the lens. As a first step, we do not attempt to model the gravitational arcs and fit only the light of the lensing objects. This is used as a starting point for all other lens models. We note that this parametric reconstruction of the lens light is not completely sufficient to model accurately the inner part of the system. SDSS J0919 + 2720 has

a very complex luminous structure, probably due to absorption by dust. However, this occurs only in the central part of the lens galaxy, so we place a mask of 0.84" in diameter at the centre of the frame.

The gravitational arcs are modelled using a PEMD profile at the position of the main galaxy, along with external shear. The main lens galaxy is a massive early-type galaxy similar in terms of morphology, lensing mass and redshift to the lens galaxies of the Sloan Lens Advanced Camera for Surveys survey³¹. We expect that the main deflector also shares a comparable mass profile. Consequently, we adopt a Gaussian prior on the logarithmic slope, $\gamma_1 = 2.08 \pm 0.13$, measured by Shajib et al.³² on the Sloan Lens Advanced Camera for Surveys galaxies. We use a Sérsic light profile superimposed onto a set of shapelets^{33,34} for the source galaxy and fix $n_{\text{max}} = 8$ as the maximum order of the shapelet basis. This ensures good source reconstruction of the small-scale features at a fairly low computation cost. In our baseline model, we place an SIE at the position of the quasar. This is required to fit the gravitational arcs down to the noise level and improves the BIC by 234 as compared with a model without this substructure (Table 1). The corresponding Einstein radius is directly inferred within a Bayesian framework and later converted into an estimate of the mass within it via the lensing relation

$$\theta_E = \sqrt{\frac{4GM(\theta < \theta_E) D_{\text{ls}}}{c^2 D_l D_s}}, \quad (1)$$

where D_l is the angular diameter distance to the lens, D_s is the distance to the source, D_{ls} is the distance between the lens and the source, $M(\theta < \theta_E)$ is the mass enclosed within the Einstein radius, G is the gravitational constant and c is the speed of light.

Pixelated source reconstruction

As an alternative to the reconstruction with shapelets and to further refine the source model, we performed a pixelated reconstruction of the source by using the Python package *SLITronomy*^{21,35}, from our best lens model. The source pixel values are regularized using priors based on sparsity, wavelet transforms and positivity constraint. The optimization of the cost function uses automatic differentiation. We use two types of wavelets including starlets, which are a set of basis functions that have been shown to be particularly suitable to represent the light profile of astronomical objects³⁶. The multi-resolution properties of the wavelets allow us to capture small-scale features in the light profile that can not be fully modelled with shapelets. In addition, it ensures that the reconstructed source image contains only pixel values that are 3σ above the noise level (see ref. 21 for details). This technique allows us to provide high-resolution de-lensed images of the source galaxy located at a redshift of $z_s = 0.558$. The reconstruction is done separately in each band, and we use the combination of the available bands to produce the colour image of the source galaxy shown in Fig. 1 (bottom right). Also, Supplementary Fig. 1 shows our best lens model, as well our shapelets and pixelated source reconstruction for each individual HST band.

Black hole mass estimation

Spectroscopic observations of SDSS J0919 + 2720 are available from the SDSS seventh data release³⁷ and from Keck/LRIS¹. The broad H α , H β and [OIII] emission lines of the quasar are visible in these data, making it possible to measure the redshift of the quasar ($z_l = 0.209$). Also detected are the [OIII] and [OII] emission lines of the background star-forming galaxy at $z_s = 0.558$, in both the SDSS and Keck/LRIS spectra.

To obtain an estimate of the black hole mass, we first subtract the host component from the SDSS and Keck spectra by using *pyQSOfit*³⁸, which enables modelling of the host using principal component analysis (PCA) based on the host components from ref. 39. In practice, rest-frame data below 3,450 Å are ignored when the host decomposition is performed because the basis eigenvectors from the PCA are not available at bluer wavelengths. We also correct for galactic extinction

based on the extinction maps of Schlegel et al.⁴⁰. This is generally a small correction, that is, amounting to less than 20% of the flux at the wavelength of H α , but it matters for getting a more reliable host–QSO decomposition. Once a reliable host–QSO decomposition is achieved, we perform a local fit of the H α (which has better signal-to-noise ratio than H β) on the host-corrected spectra. The result of this fit is shown in Supplementary Fig. 2. We considered the following two data sets: (1) the SDSS spectrum, which is relatively noisy but properly calibrated in flux (where the fibre is 3" in diameter and therefore contains a large fraction of the host) and (2) the Keck long-slit spectrum published in ref. 1, which contains a smaller fraction of the host but is only corrected for the instrumental response curve. Therefore, we obtain the black hole mass from the FWHM of the broad H α line measured using both the Keck and SDSS spectra and from the quasar luminosity derived only from SDSS. For the local fit of H α , we perform a local fit of the continuum, and fit narrow emission lines for H α , and for the [NII] doublet. The separations between those three lines are forced to match the theoretical one, while their width is assumed to be identical. An additional broad component is assumed for H α , but its zero velocity is not forced to be at the systemic velocity. A small offset by 40 km s⁻¹ with respect to the systemic redshift is effectively measured. The scaling relation used to derive the black hole mass is the one proposed for a local fitting procedure presented in ref. 41:

$$M_{\text{BH}} = K(L_{\lambda})^{\alpha} (\text{FWHM})^2, \quad (2)$$

with L in units of 10⁴⁴ erg s⁻¹ and FWHM in units of 1,000 km s⁻¹. For the H α line, we have $\log(K) = 6.779$ and $\alpha = 0.634$. We use the luminosity at 6,200 Å derived from the de-reddened and host-corrected SDSS spectrum.

We find a black hole mass of $\log(M_{\text{BH}}/M_{\odot}) = 7.29$ from the SDSS spectrum and $\log(M_{\text{BH}}/M_{\odot}) = 7.32$ from the Keck/LRIS data (Supplementary Table 1). We adopt a conservative error of 0.35 dex, corresponding to the intrinsic scatter of the relation, which dominates over the other sources of error. These estimates are in good agreement with the estimates from Liu et al.⁴², who derived $\log(M_{\text{BH}}/M_{\odot}) = 7.15$ from the H β line and $\log(M_{\text{BH}}/M_{\odot}) = 7.20$ from H α using the relation described in ref. 43.

We note that the FWHM derived for H α from the local fit depends little on the data quality or the host correction. We find agreement within 100 km s⁻¹ between the SDSS and Keck spectra, the host spectrum being subtracted or not. We note here that, while the PCA predicts emission/absorption at the level of the H α line, only flat continuum emission is subtracted, such that our H α model effectively models narrow emission from the host and from the AGN's narrow line region.

Stellar mass estimation and modelling of the stellar velocity dispersion

Photometric measurements of the quasar host galaxy come as a by-product of our lens modelling procedure. To ensure that the best fit of the lens light components is reached, we remove the central mask from our baseline model and rerun the optimization with all degrees of freedom in the lens light models, in addition to all the mass and source parameters. We optimize a total of 103 linear parameters and 62 non-linear parameters. When all pixels are included in the calculation of the likelihood, we observe a marginal change of the posterior distribution of the lens mass parameters and we find $\log_{10}(M_{\text{Tot,h}}/M_{\odot}) = 10.23^{+0.03}_{-0.03}$, well compatible with the estimate from our baseline model.

From this model, we extract the photometry of the host within an aperture of 0.71" in diameter using the double Sérsic model fitted to the HST images. In doing so, contamination by the main lens galaxy, by the lensed source and by the quasar are removed. Using the HST zero point for photometric calibration, we obtain a magnitude of 20.33 and 21.41 in the F814W and F475W band, respectively. For comparison, the magnitude of the quasar, modelled as a point source, is 20.88 and

21.89 in the F814W and F475W band, respectively. The luminosity ratio between the quasar and its host galaxy is therefore around 0.6 in both bands. We adopt a conservative photometric error of 0.2 mag on these estimates before proceeding to a fit of the spectral energy distribution of the quasar host galaxy. This reflects the worst measured discrepancy between the full lens modelling photometry and the aperture photometry of the host performed on the PSF-subtracted HST data.

The stellar mass of the quasar host galaxy, $M_{\star,h}$, is inferred by using the SED fitting package GSF (<https://github.com/mtakahiro/gsf>)⁴⁴, adopting a range of stellar ages up to 10.0 Gyr and solar metallicity. A single-colour measurement is not really sufficient to constrain the stellar template, the star formation rate, the age and the metallicity, but the quantity we are interested in, that is, the stellar mass, is mostly constrained by the normalization of the stellar template, which is well measured in our two filters. Our best fits to the measured flux in each of the two HST bands are obtained for stellar population aged 5.2, 4.7 and 4.5 Gyr, that is, $\log_{10}(M_{\star,h}/M_{\odot}) = 10.10$, $\log_{10}(M_{\star,h}/M_{\odot}) = 9.80$ and $\log_{10}(M_{\star,h}/M_{\odot}) = 9.81$ for Salpeter, Chabrier and Kroupa IMF, respectively. The uncertainty of $M_{\star,h}$ is estimated to be 0.2 dex (refs. 9,15,45) and includes the uncertainties due to the age/metallicity degeneracy⁴⁶. Changing the metallicity from solar metallicity Z_{\odot} to $0.5Z_{\odot}$ or $1.6Z_{\odot}$ changes the central value of our mass estimates by less than 0.1 dex.

We repeat this procedure to estimate the stellar mass of the main galaxy, $M_{\star,m}$. This time, we remove the light components originating from the quasar and the quasar host galaxy before measuring the flux within an aperture of 2.03", corresponding to twice the Einstein radius of the main lens. We obtain a magnitude of 18.50 and 20.62 in the F814W and F475W band, respectively. This translates to a stellar mass of $\log_{10}(M_{\star,m}/M_{\odot}) = 10.84$, $\log_{10}(M_{\star,m}/M_{\odot}) = 10.72$ and $\log_{10}(M_{\star,m}/M_{\odot}) = 10.75$, and stellar age of 7.8, 9.5 and 10.0 Gyr for Salpeter, Chabrier and Kroupa IMF, respectively.

Finally, the lens model of SDSS J0919 + 2720 allows us to estimate the stellar velocity dispersion of both the main and quasar host galaxy. Here, we assume that the motion of the stars is isotropic within the Einstein radius of each mass component. From spherical Jeans modelling, we obtain a luminosity (F814W)-weighted line-of-sight velocity dispersion (see, for example, refs. 22,47) for the quasar host galaxy of $\sigma_{\star,h} = 111 \pm 3$ km s⁻¹, within an aperture of 0.71", corresponding to the Einstein radius. For the main galaxy, we estimate the luminosity-weighted line-of-sight velocity dispersion to be $\sigma_{\star,m} = 227 \pm 3$ km s⁻¹, within an aperture of 2.03" and in the F814W filter. Note that these estimates are only indicative as they reflect the conversion of the lensing total mass in terms of dynamics.

Lens modelling robustness checks

Mass model assumptions. We verify that the mass estimate of the quasar host galaxy is robust against the assumptions made on the mass profile of the main lens galaxy and on the quasar host. From our baseline model, composed of a PEMD for the main galaxy and of an SIE for the quasar host, we tested whether the fit is improved by relaxing the slope of the mass profile of the quasar host. The imaging reduced χ^2_{img} is indeed slightly improved by $\Delta\chi^2_{\text{img}} = -1.08 \times 10^{-4}$, but the introduction of an extra degree of freedom degrades the BIC (with a ΔBIC of 4). The estimated mass within the Einstein radius of the host galaxy for these two models still remains compatible within approximately 0.5σ . We perform similar tests for different mass modelling assumptions of the main galaxy (SIE or PEMD) and for the quasar host (SIE, PEMD and point mass). Table 1 summarizes the inferred host mass, the BIC and the imaging χ^2_{img} of each of these modelling choices. Using the BIC as a proxy for Bayesian evidence, we can combine the six models of Table 1 which include the quasar host galaxy, weighted by their BIC. This gives $\log_{10}(M_{\text{Tot,h}}/M_{\odot}) = 10.27^{+0.07}_{-0.07}$, which is very similar to our baseline estimate. The weights attributed to each model are 1.00 for the first model (PEMD + SIE), 0.135 for the second model (PEMD + PEMD), 0.011 for the third model (SIE + SIE) and 0 for the other three models.

In our baseline model, perturbations of the lensing potential introduced by any object not explicitly modelled are captured by external shear. The only bright object not explicitly in our model is the companion galaxy at the south-east of the main lens galaxy. If we explicitly include it in our models, assuming it is at the same redshift as the quasar, we find its mass to be $\log_{10}(M_{\text{comp}}/M_{\odot}) < 8.41$ at a 99% confidence level (CL). The mass estimate of the host galaxy remains compatible with our baseline model within 1σ . Additionally, we test the possibility of adding a point mass at the position of the quasar on top of a non-singular isothermal ellipsoid (NIE) to model the central black hole atop a cored bulge component. The data constrain the core size of the NIE to $r_{\text{core}} < 0.30$ kpc at a 99% CL. We also obtain an upper limit for the point mass model representing the central black hole $\log_{10}(M_{\text{BH}}/M_{\odot}) < 9.03$ at a 99% CL.

Light traces mass assumption. We verify here that the light and mass profiles share the same centroids. To do this, we relax the assumption that light traces mass in our baseline model and optimize all the model parameters while assuming independent centroids for the mass and light profiles of both the main lens and the quasar host galaxy. The posterior distribution of a subset of the modelling parameters is shown in Supplementary Fig. 3.

When the centres of the mass profiles are allowed to vary during the fit, they naturally tend to align with the position of the light profiles within uncertainties. The inferred mass of the host is, with no surprise, less precise by 0.07 dex, $\log_{10}(M_{\text{Tot,h}}/M_{\odot}) = 10.17 \pm 0.14$, but remains compatible with our baseline model within 1σ uncertainties. This leaves all our conclusions unchanged and indicates that the light and mass distributions of the different components in our models share the same centroid.

Data availability

The HST images supporting this work are publicly available on the Hubble Legacy Archive (<https://hla.stsci.edu/>). Our reduced Keck and SDSS spectra are available on Zenodo (<https://doi.org/10.5281/zenodo.7806468>).

Code availability

The lens modelling code `Lenstronomy` and the source reconstruction software `SLITronomy` are freely accessible at <https://github.com/sibirrer/lenstronomy> and <https://github.com/aymgal/SLITronomy>. Stellar masses were estimated by using the public python package `GSF` (<https://github.com/mtakahiro/gsf>). The HST PSF was reconstructed using `AstroObjectAnalyser`, which is publicly available at <https://github.com/sibirrer/AstroObjectAnalyser>. Spectra have been fitted using `pyQSOfit`, which is also publicly available at <https://github.com/legolason/PyQSOfit>.

References

- Courbin, F. et al. Three quasi-stellar objects acting as strong gravitational lenses. *Astron. Astrophys.* **540**, A36 (2012).
- Ferrarese, L. & Merritt, D. A fundamental relation between supermassive black holes and their host galaxies. *Astrophys. J.* **539**, L9–L12 (2000).
- Gebhardt, K. et al. A relationship between nuclear black hole mass and galaxy velocity dispersion. *Astrophys. J.* **539**, L13–L16 (2000).
- Springel, V. et al. Simulations of the formation, evolution and clustering of galaxies and quasars. *Nature* **435**, 629–636 (2005).
- Di Matteo, T., Colberg, J., Springel, V., Hernquist, L. & Sijacki, D. Direct cosmological simulations of the growth of black holes and galaxies. *Astrophys. J.* **676**, 33–53 (2008).
- Peng, C. Y. How mergers may affect the mass scaling relation between gravitationally bound systems. *Astrophys. J.* **671**, 1098–1107 (2007).
- Kormendy, J. & Ho, L. C. Coevolution (or not) of supermassive black holes and host galaxies. *Annu. Rev. Astron. Astrophys.* **51**, 511–653 (2013).
- Sexton, R. O. et al. Stronger constraints on the evolution of the $M_{\text{BH}}-\sigma_*$ relation up to $z \sim 0.6$. *Astrophys. J.* **878**, 101 (2019).
- Ding, X. et al. The mass relations between supermassive black holes and their host galaxies at $1 < z < 2$ HST-WFC3. *Astrophys. J.* **888**, 37 (2020).
- Ding, X. et al. Testing the evolution of correlations between supermassive black holes and their host galaxies using eight strongly lensed quasars. *Mon. Not. R. Astron. Soc.* **501**, 269–280 (2021).
- Jahnke, K. et al. Massive galaxies in COSMOS: evolution of black hole versus bulge mass but not versus total stellar mass over the last 9 Gyr? *Astrophys. J.* **706**, L215–L220 (2009).
- Schramm, M. & Silverman, J. D. The black hole-bulge mass relation of active galactic nuclei in the Extended Chandra Deep Field-South Survey. *Astrophys. J.* **767**, 13 (2013).
- Schulze, A. & Wisotzki, L. Accounting for selection effects in the BH–bulge relations: no evidence for cosmological evolution. *Mon. Not. R. Astron. Soc.* **438**, 3422–3433 (2014).
- Woo, J. H. in *Panoramic Views of Galaxy Formation and Evolution*, vol. 399 (eds Kodama, T., Yamada, T. & Aoki, K.) (Astronomical Society of the Pacific, 2008).
- Treu, T., Woo, J.-H., Malkan, M. A. & Blandford, R. D. Cosmic evolution of black holes and spheroids. II. Scaling relations at $z = 0.36$. *Astrophys. J.* **667**, 117–130 (2007).
- Cen, R. Coevolution between supermassive black holes and bulges is not via internal feedback regulation but by rationed gas supply due to angular momentum distribution. *Astrophys. J. Lett.* **805**, L9 (2015).
- Lauer, T. R., Tremaine, S., Richstone, D. & Faber, S. M. Selection bias in observing the cosmological evolution of the $M_{\text{BH}}-\sigma$ and $M_{\text{BH}}-L$ relationships. *Astrophys. J.* **670**, 249–260 (2007).
- Claeskens, J. F., Lee, D. W., Remy, M., Sluse, D. & Surdej, J. QSO mass constraints from gravitational lensing studies of quasar pairs. The cases of Q1548+114 A & B and Q1148+0055 A & B. *Astron. Astrophys.* **356**, 840–848 (2000).
- Meyer, R. A., Delubac, T., Kneib, J.-P. & Courbin, F. Quasi-stellar objects acting as potential strong gravitational lenses in the SDSS-III BOSS survey. *Astron. Astrophys.* **625**, A56 (2019).
- Taak, Y. C. & Im, M. High- z Universe probed via lensing by QSOs (HULQ). I. Number estimates of QSO–QSO and QSO–galaxy lenses. *Astrophys. J.* **897**, 163 (2020).
- Galan, A., Peel, A., Joseph, R., Courbin, F. & Starck, J. L. SLITRONOMY: towards a fully wavelet-based strong lensing inversion technique. *Astron. Astrophys.* **647**, A176 (2021).
- Suyu, S. H. et al. Dissecting the gravitational lens B1608+656. II. Precision measurements of the Hubble constant, spatial curvature, and the dark energy equation of state. *Astrophys. J.* **711**, 201–221 (2010).
- Despali, G. et al. Detecting low-mass haloes with strong gravitational lensing I: the effect of data quality and lensing configuration. *Mon. Not. R. Astron. Soc.* **510**, 2480–2494 (2022).
- Grier, C. J. et al. Stellar velocity dispersion measurements in high-luminosity quasar hosts and implications for the AGN black hole mass scale. *Astrophys. J.* **773**, 90 (2013).
- Letawe, G. et al. On-axis spectroscopy of the host galaxies of 20 optically luminous quasars at $z \sim 0.3$. *Mon. Not. R. Astron. Soc.* **378**, 83–108 (2007).
- Millon, M. et al. TDCOSMO. I. An exploration of systematic uncertainties in the inference of H_0 from time-delay cosmography. *Astron. Astrophys.* **639**, A101 (2020).
- Park, D. et al. Extending the calibration of C IV-based single-epoch black hole mass estimators for active galactic nuclei. *Astrophys. J.* **839**, 93 (2017).

28. Bahk, H., Woo, J.-H. & Park, D. Calibrating Mg II-based black hole mass estimators with H β reverberation measurements. *Astrophys. J.* **875**, 50 (2019).
29. Bertin, E. & Arnouts, S. SExtractor: software for source extraction. *Astron. Astrophys. Suppl. Ser.* **117**, 393–404 (1996).
30. Birrer, S. et al. lenstronomy II: A gravitational lensing software ecosystem. *J. Open Source Softw.* **6**, 3283 (2021).
31. Bolton, A. S., Burles, S., Koopmans, L. V. E., Treu, T. & Moustakas, L. A. The Sloan Lens ACS Survey. I. A large spectroscopically selected sample of massive early-type lens galaxies. *Astrophys. J.* **638**, 703–724 (2006).
32. Shajib, A. J., Treu, T., Birrer, S. & Sonnenfeld, A. Dark matter haloes of massive elliptical galaxies at $z \sim 0.2$ are well described by the Navarro–Frenk–White profile. *Mon. Not. R. Astron. Soc.* **503**, 2380–2405 (2021).
33. Refregier, A. Shapelets - I. A method for image analysis. *Mon. Not. R. Astron. Soc.* **338**, 35–47 (2003).
34. Birrer, S., Amara, A. & Refregier, A. Gravitational lens modeling with basis sets. *Astrophys. J.* **813**, 102 (2015).
35. Joseph, R., Courbin, F., Starck, J. L. & Birrer, S. Sparse lens inversion technique (SLIT): lens and source separability from linear inversion of the source reconstruction problem. *Astron. Astrophys.* **623**, A14 (2019).
36. Starck, J.-L., Fadili, J. & Murtagh, F. The undecimated wavelet decomposition and its reconstruction. *IEEE Trans. Image Process.* **16**, 297–309 (2007).
37. Abazajian, K. N. et al. The seventh data release of the Sloan Digital Sky Survey. *Astrophys. J. Suppl.* **182**, 543–558 (2009).
38. Guo, H., Shen, Y. & Wang, S. PyQSOFit: Python code to fit the spectrum of quasars (Astrophysics Source Code Library, 2018); <http://ascl.net/1809.008>
39. Yip, C. W. et al. Spectral classification of quasars in the Sloan Digital Sky Survey: eigenspectra, redshift, and luminosity effects. *Astron. J.* **128**, 2603–2630 (2004).
40. Schlegel, D. J., Finkbeiner, D. P. & Davis, M. Maps of dust infrared emission for use in estimation of reddening and cosmic microwave background radiation foregrounds. *Astrophys. J.* **500**, 525–553 (1998).
41. Mejía-Restrepo, J. E., Trakhtenbrot, B., Lira, P., Netzer, H. & Capellupo, D. M. Active galactic nuclei at $z \sim 1.5$ – II. Black hole mass estimation by means of broad emission lines. *Mon. Not. R. Astron. Soc.* **460**, 187–211 (2016).
42. Liu, H.-Y. et al. A comprehensive and uniform sample of broad-line active galactic nuclei from the SDSS DR7. *Astrophys. J. Suppl.* **243**, 21 (2019).
43. Ho, L. C. & Kim, M. A revised calibration of the virial mass estimator for black holes in active galaxies based on single-epoch H β spectra. *Astrophys. J.* **809**, 123 (2015).
44. Morishita, T. et al. Massive dead galaxies at $z \sim 2$ with HST Grism spectroscopy. I. Star formation histories and metallicity enrichment. *Astrophys. J.* **877**, 141 (2019).
45. Park, D. et al. Cosmic evolution of black holes and spheroids. V. The relation between black hole mass and host galaxy luminosity for a sample of 79 active galaxies. *Astrophys. J.* **799**, 164 (2015).
46. Bell, E. F. & de Jong, R. S. Stellar mass-to-light ratios and the Tully–Fisher relation. *Astrophys. J.* **550**, 212–229 (2001).
47. Binney, J. & Tremaine, S. *Galactic Dynamics* (Princeton University Press, 1987).
48. Häring, N. & Rix, H.-W. On the black hole mass–bulge mass relation. *Astrophys. J.* **604**, L89–L92 (2004).
49. Bennert, V. N., Auger, M. W., Treu, T., Woo, J.-H. & Malkan, M. A. A local baseline of the black hole mass scaling relations for active galaxies. I. Methodology and results of pilot study. *Astrophys. J.* **726**, 59 (2011).

Acknowledgements

M.M. acknowledges the support of the Swiss National Science Foundation (SNSF) under grant P500PT_203114. M.M., F.C. and A.G. are supported by the European Research Council (ERC) under the European Union’s Horizon 2020 research and innovation programme (COSMICLENS: grant agreement no. 787886) and the Swiss National Science Foundation (SNSF) under grant 200020_200463. X.D. is supported by JSPS KAKENHI grant no. JP22K14071.

Author contributions

M.M. conducted the analysis. A.G. developed the source reconstruction algorithm SLITronomy. M.M. and F.C. wrote the manuscript. X.D. did the stellar population analysis. D.S. measured the black hole mass. All other co-authors actively participated in the discussions, in the HST data acquisition and in the discovery process of SDSS J0919+2720.

Competing interests

The authors declare no competing interest.

Additional information

Supplementary information The online version contains supplementary material available at <https://doi.org/10.1038/s41550-023-01982-2>.

Correspondence and requests for materials should be addressed to Martin Millon.

Peer review information *Nature Astronomy* thanks the anonymous reviewers for their contribution to the peer review of this work.

Reprints and permissions information is available at www.nature.com/reprints.

Publisher’s note Springer Nature remains neutral with regard to jurisdictional claims in published maps and institutional affiliations.

Springer Nature or its licensor (e.g. a society or other partner) holds exclusive rights to this article under a publishing agreement with the author(s) or other rightsholder(s); author self-archiving of the accepted manuscript version of this article is solely governed by the terms of such publishing agreement and applicable law.

© The Author(s), under exclusive licence to Springer Nature Limited 2023